

Energetics and diffusion of gold in bismuth telluride

M. C. Shaughnessy,¹ J.D. Sugar,¹ N. C. Bartelt,¹ and J. A. Zimmerman¹

¹*Sandia National Laboratories, Livermore, CA 94551*

(Dated: May 3, 2013)

In this paper, we use high-temperature experiments coupled with *ab-initio* modeling of diffusion to study Au in Bi₂Te₃. This combined methodology enables us to elucidate key aspects of the mechanisms of diffusion and the solubility behavior of the Au-Bi₂Te₃ system. Using electron microscopy and energy dispersive spectroscopy, we observe fast motion of Au into Bi₂Te₃ and concentrations above the previously reported solubility limit, sufficient to deplete many microns of Au on the Bi₂Te₃ surface after 165 hours at 350°C. We calculate defect formation energies and diffusion barriers within DFT to develop an atomistic understanding of fluxes of Au into Bi₂Te₃. We identify an interstitial mechanism responsible for the observed rapid anisotropic diffusion and provide an estimate of the heat of transport, Q^* , associated with temperature-gradient driven diffusion. The calculated diffusivity along the Te-Te double layer plane is in good agreement with experiment, while the much slower cross-plane diffusivity requires a non-interstitial mechanism. The low formation energies of substitutional defects suggest these types of defects may be active during diffusion and may explain the high observed concentrations.

Key Words: thermoelectric, bismuth telluride, contact, diffusion

PACS numbers:

INTRODUCTION

Bismuth telluride, Bi₂Te₃, is a narrow bandgap semiconductor commonly used for waste heat harvesting and electrical cooling[1] due to its large thermoelectric figure of merit, ZT. Recent interest in this material has been driven by the prospect of improving ZT through nanostructuring[2–4], as well as by the discovery of topologically protected, highly mobile electronic surface states in Bi₂Te₃ and related compounds, such as Bi₂Se₃ and Bi_xSb_{1-x}[5, 6]. Both thermoelectric and topological insulator properties involve somewhat electrical transport, so understanding the properties of metal contacts to Bi₂Te₃ could facilitate further scientific and technological advances with this material.

Bi₂Te₃ possesses a layered, trigonal structure based on that of tetradymite[7, 8]. Quintuple layers of Te⁽¹⁾-Bi-Te⁽²⁾-Bi-Te⁽¹⁾ are stacked in the z-direction, as shown in Fig. 1. The mixture of covalent bonding within the quintuple layers and van der Waals bonding between them creates an exceptionally varied, and variable, electrical environment for defects and transport of atoms and electrons. Features of both bulk and surface environments are simultaneously present.

Various contact metals have been used in Bi₂Te₃ devices, including Pt[9], Ag[10], and Au[11, 12]. Au and Au/Ti layers[13] form good electrical contacts with acceptable mechanical properties. In electrical devices with Au electrodes there is fast diffusion from the electrode into the Bi₂Te₃ region[12]. Seminal measurements of diffusivity and solubility of Au in Bi₂Te₃ were carried out by Keys and Dutton[14], who found exceptionally fast diffusion in single crystal specimens parallel to the Te-Te double layer planes, Au solubility (about 10¹⁸ atoms/cm³ at 300K, much lower than that of commonly used dopants in thermoelectric applications), and hardening. Although the mechanism responsible for the high diffusivity is unknown, the diffusion mechanisms for Cu[15], Ag[16, 17] and Se [18] in Bi₂Te₃ have been investigated. In the latter case, a mechanism involving antisite defects and thermal vacancies was proposed. In the former studies involving the metals, electron-ion interactions were thought to be relevant, partially due to the large carrier concentration ($\sim 10^{19}$ /cm³) at room temperature due to intrinsic doping. Rapid diffusion in the plane formed by the weakly bound Te-Te double layers was suggested for Au, Cu and Ag, but there exists considerable uncertainty regarding the diffusion mechanism.

Although the measured solubility is low, the importance of doping in thermoelectric[19–21] and topological insulator[22, 23] applications as well as the more general question of aging in electrically contacted thermoelectric devices motivate us to understand the detailed atomistic mechanism of Au incorporation and transport in Bi₂Te₃. In this paper we describe experiments to observe Au diffusion into polycrystalline n- and p-type Bi₂Te₃. We observe fluxes large enough to completely deplete the several microns thick Au thin films.

The possibility of reaching a high impurity concentration raises the prospect of significant degradation of the electrical and mechanical properties of Au-contacted Bi₂Te₃ over long periods of time. Furthermore, because thermoelectric devices are designed to be exposed to large temperature gradients, the Soret effect (migration driven by a temperature gradient) may also cause large concentrations of Au to accumulate in the Bi₂Te₃ devices.

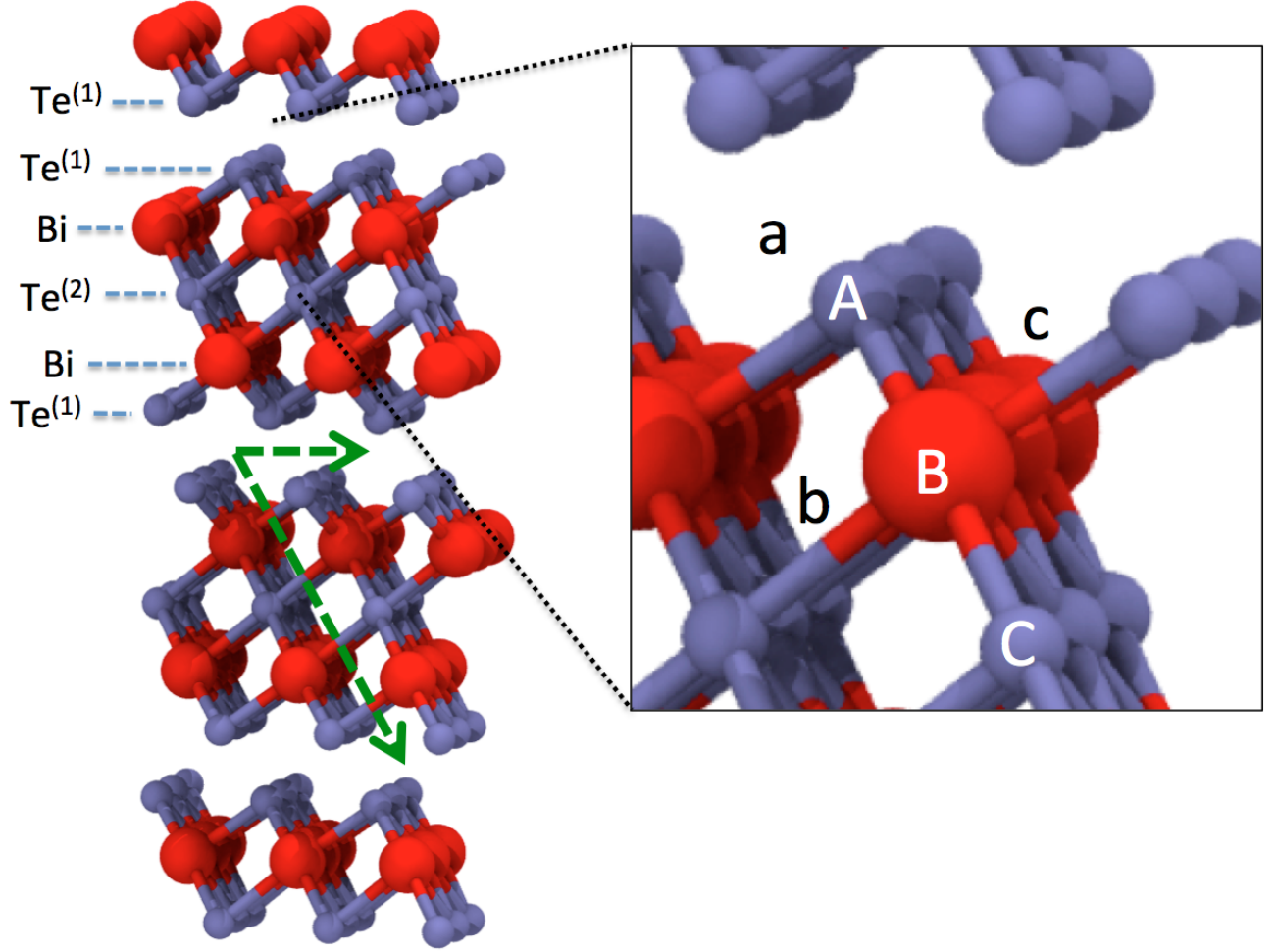


FIG. 1: The 135-atom Bi_2Te_3 unit cell with Te atoms as small purple spheres and Bi atoms as large red spheres. The substitutional doping sites are labeled in capital: $\text{Au}_{\text{Te}(1)}$ (A), Au_{Bi} (B) and $\text{Au}_{\text{Te}(2)}$ (C). The three possible interstitial sites are labeled in lowercase: $\text{Te}^{(1)}\text{-Te}^{(1)}$ int (a), $\text{Bi-Te}^{(2)}$ int (b), $\text{Bi-Te}^{(1)}$ int (c). The in-plane (shorter arrow) and out-of-plane (longer arrow) diffusion pathways are indicated by the dashed arrows in the lower portion of the supercell.

In this paper we also compute the formation energies of isolated defects and diffusivities in order to understand the observed incorporation of Au in Bi_2Te_3 . We provide an explanation of the experimental technique to observe the Au diffusion motivating the modeling. Through formation energies we address the question of which types of defects will be present. By determining a likely microscopic diffusion mechanism, we point out the origin of the observed anisotropic, rapid diffusion and also estimate the heat of transport. These quantities determine how quickly and how much the Au from a contact will be incorporated into a Bi_2Te_3 . Our calculations suggest a second slower stage of diffusion associated with Au substitution in the Bi_2Te_3 occurs after the initial rapid diffusion measured by Keys and Dutton. The effective diffusivity in the second stage will be kinetically limited by the availability of substitutional defect sites, and thus most difficult to observe in highly crystalline stoichiometric samples.

II. METHOD

Experiment

To perform aging experiments, Au contacts are sputter deposited onto two n-type Bi_2Te_3 substrates. The substrates are sintered and lightly doped with Se to a nominal composition of $\text{Bi}_2\text{Te}_{2.5}\text{Se}_{0.5}$, improving the thermoelectric properties when compared to undoped Bi_2Te_3 . Circular Au contacts are patterned onto the substrates for future

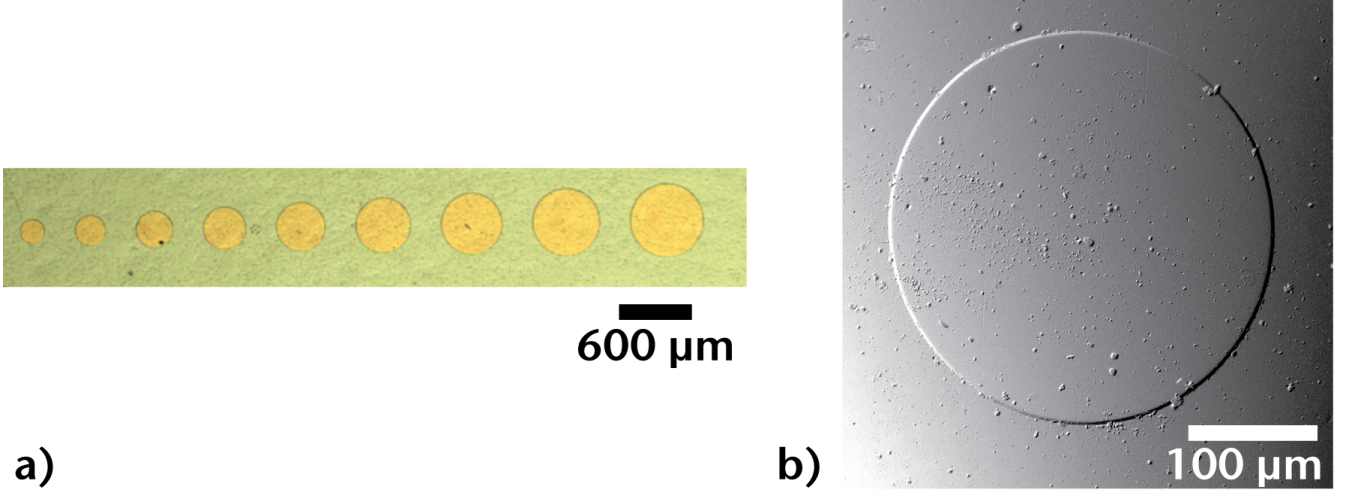


FIG. 2: The optical micrograph in a) shows a lithographically patterned Au film on N-type Bi₂Te₃. The Au circles range in diameter from 200 μm to 600 μm in steps of 50 μm . This pattern is chosen for Cox and Strack[24] contact resistance measurements, which will be discussed in subsequent work. The SEM micrograph in b) shows a single Au contact as processed. There is cutting debris on the surface because we dice a larger substrate into smaller sections.

studies of contact resistance using the Cox and Strack method[24]. Conventional UV lithography is used to pattern circles ranging in diameter from 200 to 600 μm in steps of 50 μm onto the substrate surfaces. Before depositing Au, the substrate surfaces are briefly etched with an argon plasma, and then Au is sputter deposited to a thickness of 1 μm as shown in Fig. 2. Aging is performed in evacuated quartz tubes at 150°C, 250°C, and 350°C for 65 hr and 163 hr. The Au contacts are characterized with scanning electron microscopy (JEOL 7600, JEOL 840, and PhenomWorld desktop SEM) and scanning transmission electron microscopy (JEOL 2010 FEG operating at 200 kV). EDS analysis in the TEM is performed with Digiscan scan controls (Gatan, Inc.) and a SiLi EDS detector (Oxford, Inc.).

Modeling

We use a 135-atom supercell of pure Bi₂Te₃ for density functional theory (DFT) calculations. Previous studies of native defects in Bi₂Te₃ suggest such a supercell can accurately model isolated defects [25]. The VASP code [26], with standard projector augmented wave (PAW) pseudopotentials, with d-electrons in the core, is used to compute the electronic structure. A planewave energy cutoff of 500 eV and a Monkhorst-Pack \mathbf{k} -point mesh of $2 \times 2 \times 2$ are adopted. The basis vectors and ionic positions are relaxed to determine the low energy crystal structure, whose $a = 4.35$ Å and $c = 29.84$ Å lattice constants, as well as the Te-Te layer separation (3.46 Å) are within 1% of the experimental values ($a = 4.38$ Å and $c = 30.36$ Å Te-Te distance = 3.63 Å [8, 27]). Relaxations are finished when all forces on all atoms are less than 6 meV/Å. In the subsequent doping studies, the dimensions of the supercell are held fixed and only ionic relaxations are allowed. The spin-orbit interaction is taken into account because the Bi and Te have heavy nuclei. Fig. 1 shows the pure Bi₂Te₃ crystal supercell. There are three unique crystal atom sites and two inequivalent stable interstitial sites.

We consider two types of substitutional defect. In one type a Au atom replaces a single Bi or Te atom and the replaced atom is removed entirely. In the second type a Au atom occupies a Bi or Te site and pushes the Bi or Te atom into an adjacent interstitial site. Interstitial defects are also modeled by adding an Au atom into the pure bismuth telluride supercell at one of the three possible interstitial sites with no initial displacement of any atoms.

The method of Northrup and Zhang [28] is used to compute formation energies. For an interstitial defect

$$\Delta E_f = E_{\text{doped}} - (\mu_{\text{Au}} + E_{\text{pure}}) \quad (1)$$

where E_{doped} is the total energy of the supercell with the dopant, μ_{Au} is the chemical potential for Au, computed from fcc bulk Au, and E_{pure} is the total energy of the Bi₂Te₃ supercell with no dopant. ΔE_f is the formation energy, the energy penalty to create the doped system from the pure crystals.

In the case of a substitutional defect, we assume the displaced host crystal atom (Bi or Te) is sent to a chemically well-defined reservoir. Then,

$$\Delta E_f = E_{doped} - (\mu_{Au} + E_{pure} - \mu_{Te/Bi}) \quad (2)$$

where $\mu_{Te/Bi}$ is the chemical potential of the displaced Bi or Te atom in the reservoir. If the displaced atom remains at the adjacent interstitial site we revert to Eq. 1.

In a typical Bi_2Te_3 application, such as in the active regions of a thermocouple, there could be a variety of chemical environments and hence chemical potentials. Because the Au-Bi-Te phase diagram is known [29, 30], we assume the system of Bi_2Te_3 with the Au dopant is in equilibrium with pure Au (from a contact, say) and either AuTe_2 or BiTe , depending on whether the environment is Te-rich or Bi-rich, respectively.

AuTe_2 crystalizes in the calaverite structure with a three atom unit cell[31]. The BiTe [32] structure is related to the tetradyte Bi_2Te_3 structure, with an additional Bi double layer inserted between every other $\text{Te}^{(1)}\text{-Te}^{(1)}$ double layer. There are many other Bi-rich bismuth tellurides [33]; we chose to use BiTe because both AuTe_2 and BiTe coexist with Bi_2Te_3 in region of the Au-Bi-Te phase diagram between pure Bi_2Te_3 to pure Au.

The three μ_{Au} , μ_{Bi} , μ_{Te} can be determined from the total energies of Au, AuTe_2 , BiTe , and Bi_2Te_3 . We solve the first along with either the second or the third of the equations below.

$$2\mu_{Bi} + 3\mu_{Te} = \mu_{\text{Bi}_2\text{Te}_3} \quad (3)$$

$$\mu_{Bi} + \mu_{Te} = \mu_{\text{BiTe}} \quad (4)$$

$$\mu_{Au} + 2\mu_{Te} = \mu_{\text{AuTe}_2} \quad (5)$$

where μ_{Au} , μ_{AuTe_2} , μ_{BiTe} and $\mu_{\text{Bi}_2\text{Te}_3}$ are the total energies of one formula unit of Au, AuTe_2 , BiTe , or Bi_2Te_3 , respectively. In the Bi-rich case, Eq. 3 and Eq. 4 are solved, while in the Te-rich case Eq. 3 and Eq. 5 are solved.

Since there is no ternary phase, nor a relevant BiAu phase, our choice of chemical reservoirs is nearly unique for the dilutely Au doped stoichiometric Bi_2Te_3 . We note above 116 °C, BiAu_2 is entropically stabilized [34] and so it may appear as a possible reservoir. Errors associated with neglecting this phase would likely be much smaller in real applications than those due to departures from pure Bi_2Te_3 stoichiometry, ternary dopants for altering the host electronic structure, and non-equilibrium conditions.

The activation energy for diffusion of Au in the in-plane direction between adjacent Te-Te double layer interstitial sites is calculated with the nudged elastic band method (NEB)[35]. Au can diffuse by other ways in bismuth telluride. Along with diffusion in the cross-plane or z-direction, more complicated mechanisms, such as vacancy mediated diffusion, multiple-defect diffusion or even diffusion along grain boundaries in polycrystalline samples may contribute to the experimentally measured diffusion. The calculations presented here provide a theoretical upper bound on the diffusion through single crystal Bi_2Te_3 along solely interstitial paths.

The starting point for the NEB calculations is an Au atom in the Te-Te double layer interstitial site in the 135-atom supercell. The final configuration has the Au atom moved to an adjacent Te-Te double layer interstitial site, either in the same plane or in an adjacent Te-Te double layer. Initially, a series of 16 equally-spaced atomic positions for the Au along a line connecting the initial and final Au positions are the assumed diffusion pathway. Then, forces on each of the 16 images of the isolated Au atom along the line are computed. All atoms in each of the 16 supercells relax, with the caveat that an additional fictitious force acts on each Au atom. This elastic band force is due to adjacent images of the Au atoms, keeping them separated. In this way, the Au image atoms are forbidden from simply relaxing down to the globally favored initial or final configuration sites. The forces on all the atoms, including the fictitious elastic band forces, in each of the image supercells are recomputed until self-consistent cycle is complete. In this way low-energy metastable saddle point-crossing pathways can be found in the vicinity of the initial guess for the diffusion pathway. We note that pathways involving substitutional defects will not be discovered using this method.

III. RESULTS

We observe large fluxes of Au into the Bi_2Te_3 substrate, sufficient to deplete the contact pads (see Fig. 3). The measured concentration is several times larger than the previously reported solubility limit[14] and even further above the intermediate-time net concentrations computed using the reported diffusivity (see Fig 4). The concentration of

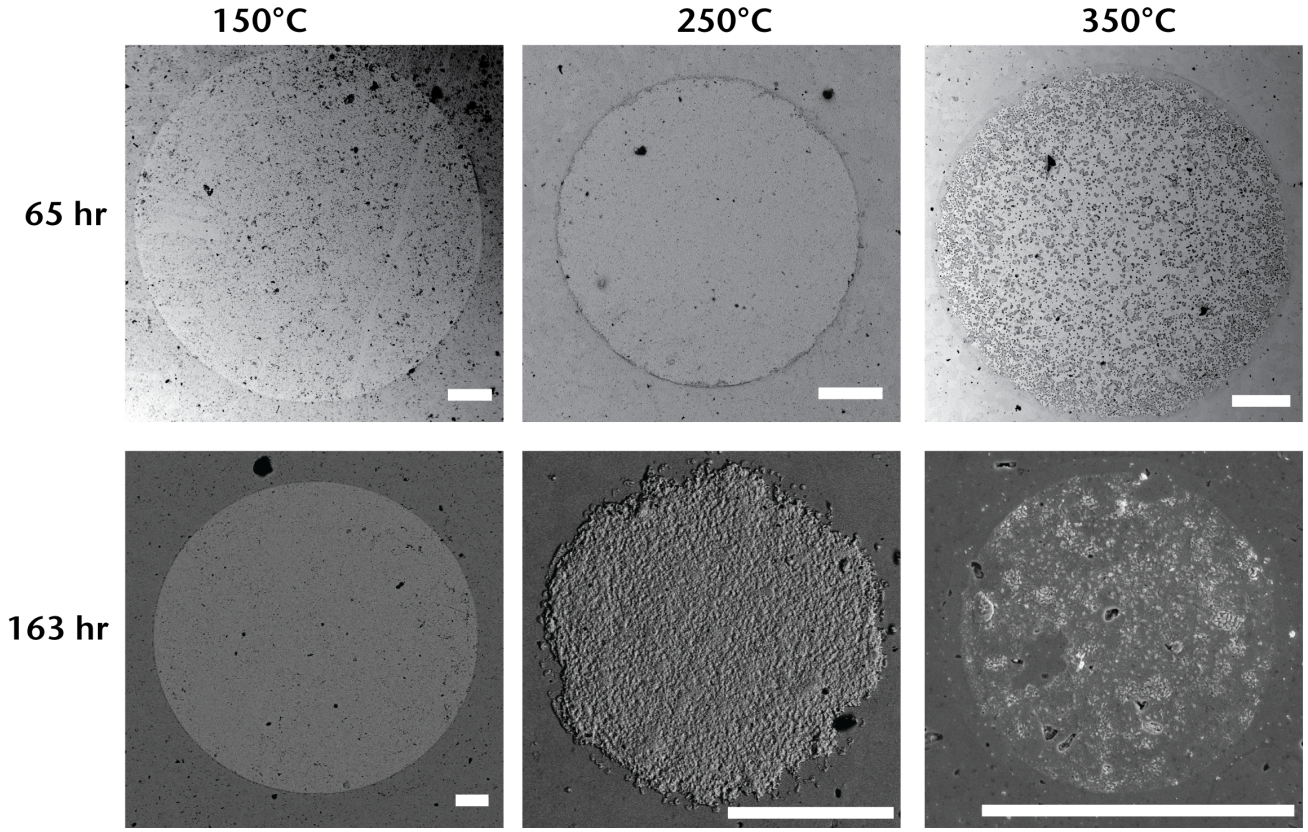


FIG. 3: The figure shows a series of Au contacts after various aging conditions (time and temperature). The scale bar in each image is $50\text{ }\mu\text{m}$ long. The Au contacts are visually intact at 150°C up to 163 hours. At 250°C there is evidence of degradation around the edges of the sample after 65 hours and roughening and degradation throughout by 163 hours. At 350°C the mostly gone by 63 hours and is practically gone after 163 hours.. Small islands remain on the surface, and EDS suggests these islands are not just pure Au, but contain Bi and Te also. At intermediate aging conditions the edges of the contact seem to disappear first. The contact develops a swiss cheese appearance with holes that open up in the middle of the contact. This is most easily visible in the image after 65 hr at 350°C .

Au in the substrate is computed by dividing the total volume of gold by the substrate volume. We fabricate two samples each with many contact pads, for total Au volumes of $4.18 \times 10^{-5}\text{cm}^3$ and $3.55 \times 10^{-5}\text{cm}^3$, corresponding to 2.47×10^{18} and 5.12×10^{18} Au atoms. The substrates are both disks 1.6 cm in diameter and 0.2 cm thick. Thus, the Au concentration in the substrate after the Au contact pads are entirely depleted is 6.13×10^{18} atoms/ cm^3 and 5.21×10^{18} atoms/ cm^3 . The greater value sets a lower limit on the solubility of Au in n-type Bi_2Te_3 higher than that measured in [14].

The STEM and EDS analysis of the contact/substrate interface shown in Fig. 5 shows changes as the Au contact diffuses into the substrate. Cavities form in both the Au and Bi_2Te_3 , suggesting both substrate and contact atoms migrate. The SEM images in Fig. 3. show pits (dark regions) in the Bi_2Te_3 substrate both under the contact and away from the contact at high temperatures and large times. This suggests the departure of Te or Bi atoms from the substrate may not be directly due to the Au contact; the Te vapor pressure of Bi_2Te_3 is exceptionally high and sublimation of Te at elevated temperatures has previously been observed. However, the EDS analysis of precipitates *on top* of the contact shows both Te and Bi migrate through the contact and precipitate. This suggests some reaction with the Au occurs. The calculations discussed next suggest substitutional Au defects are energetically cheap and the formation of substitutional Au should be kinetically limited by the cost to displace substrate Bi or Te atoms into interstitial sites. In the present Se-doped polycrystalline sample, there may be many Bi or Te vacancies or other defects whose energy can be lowered by incorporating Au into the Bi_2Te_3 .

Table 1 gives defect formation energies for interstitial, substitutional, and substitutional with displaced Bi or Te atoms. The total energy for the 135-atom pure Bi_2Te_3 model is -529.92 eV and the total energy for the bulk Au 1-atom unit cell is -3.19 eV. The lowest interstitial formation energy is the Te-Te double layer site, $\text{Te}^{(1)}\text{-Te}^{(1)}$ int, because of the relatively open structure and weak bonding between the Te-Te double layers compared to the other

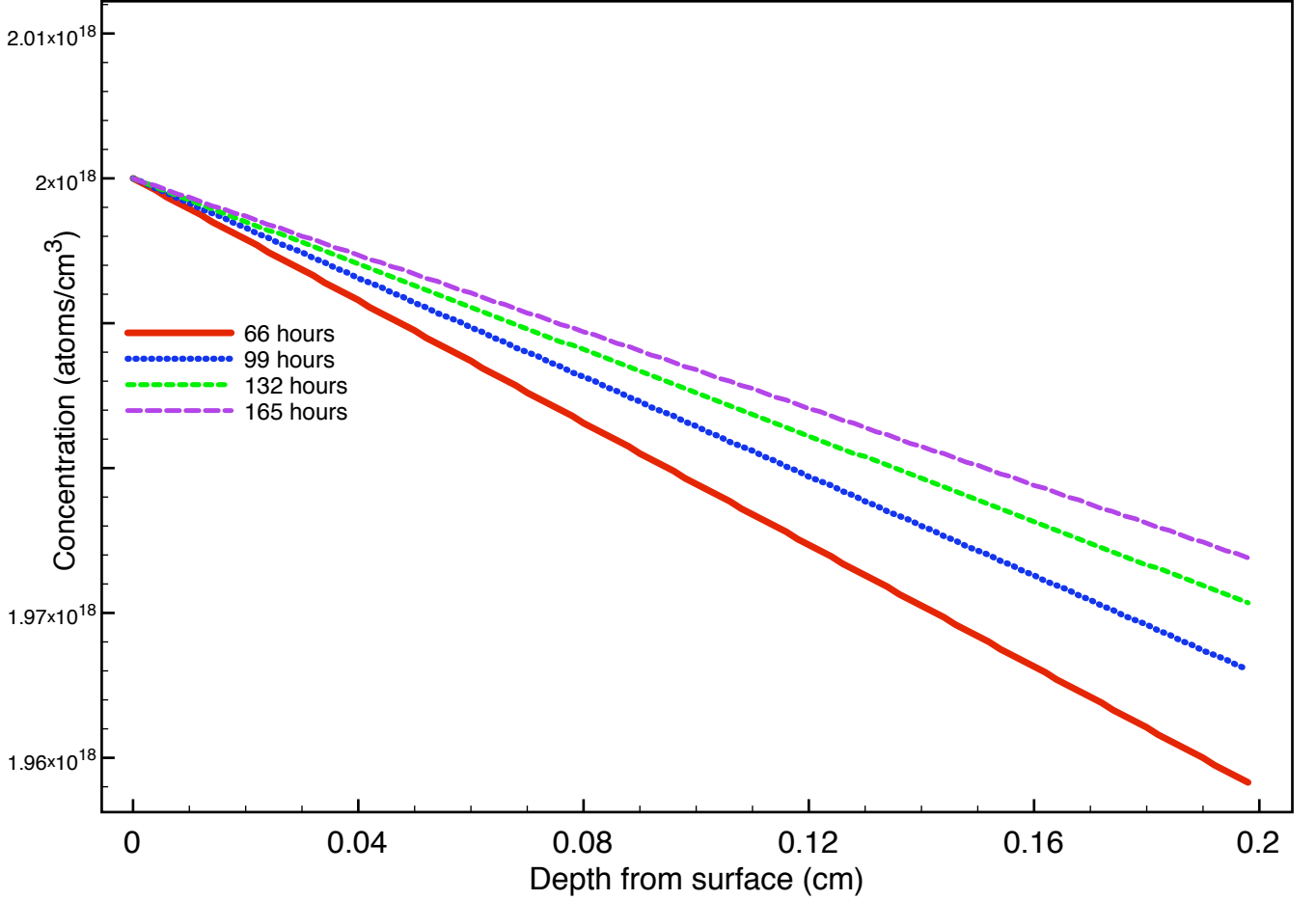


FIG. 4: The parameters provided in[14] are applied to the present experimental set up to predict the time evolution of the concentration profile, $C(x,t) = C_0 \text{erfc}(\frac{x}{\sqrt{Dt}})$. The Au flux predicted with these parameters is much less than we observed.

possible sites. Another interstitial site, the Bi-Te⁽¹⁾ int site, is unstable for Au doping. At this site the Au atom relaxes into the region between Te-Te double layer to the Te⁽¹⁾-Te⁽¹⁾ int site. The Bi-Te⁽²⁾ interstitial site formation energy is higher because the Au atom must distort more of the rigid covalent bonds present in the quintuple layer.

The simple substitutional formation energies are lower than either interstitial defect formation energy, indicating these should be more prevalent. The calculated values depend on the Bi and Te chemical potentials, but are small for both Bi-rich and Te-rich conditions. The exceptionally low formation energy for these substitutional defects might be expected after inspecting the Au-Bi-Te ternary phase diagram[30], in which several Bi-rich phases coexist with AuTe₂ and bulk Au, hinting that in the presence of Au, the Te is nearly unstable in the stoichiometric Bi₂Te₃. Recent calculations on the phonon bandstructure of AuBiTe₂ [36] suggest this compound is only weakly stable and experiments[37] show Te concentration in near-stoichiometric Bi₂Te₃ materials can be easily controlled through Te vapor pressure due to a low Te sublimation energy. This poses a problem when Bi₂Te₃ is annealed at high temperatures and the Te sublimates.

Considering the formation energies for the substitutional models with an internally displaced Te atom, their large magnitude can be understood because the displaced Te atom relaxes into the Te-Te double layer disrupting the van der Waals bonding between the Te-Te layers. The configuration with the Au substituting for a Bi and displacing the Bi into an adjacent interstitial site does not exist because it is unstable; the Bi atom returns to its crystal site and the Au relaxes into the interstitial region. The large formation energies of these substitutional-interstitial defect complexes suggests the occupation of the substitutional sites may be kinetically limited. In other words, the formation of an interstitial defect will be necessary in order to have an Au atom at a substitutional site, so even though substitution is energetically favored overall, it may take a very long time for the Au to reach the substitutional sites because of the large energy barrier. This kinetic mechanism also favors the interstitial pathway for diffusion, especially in highly

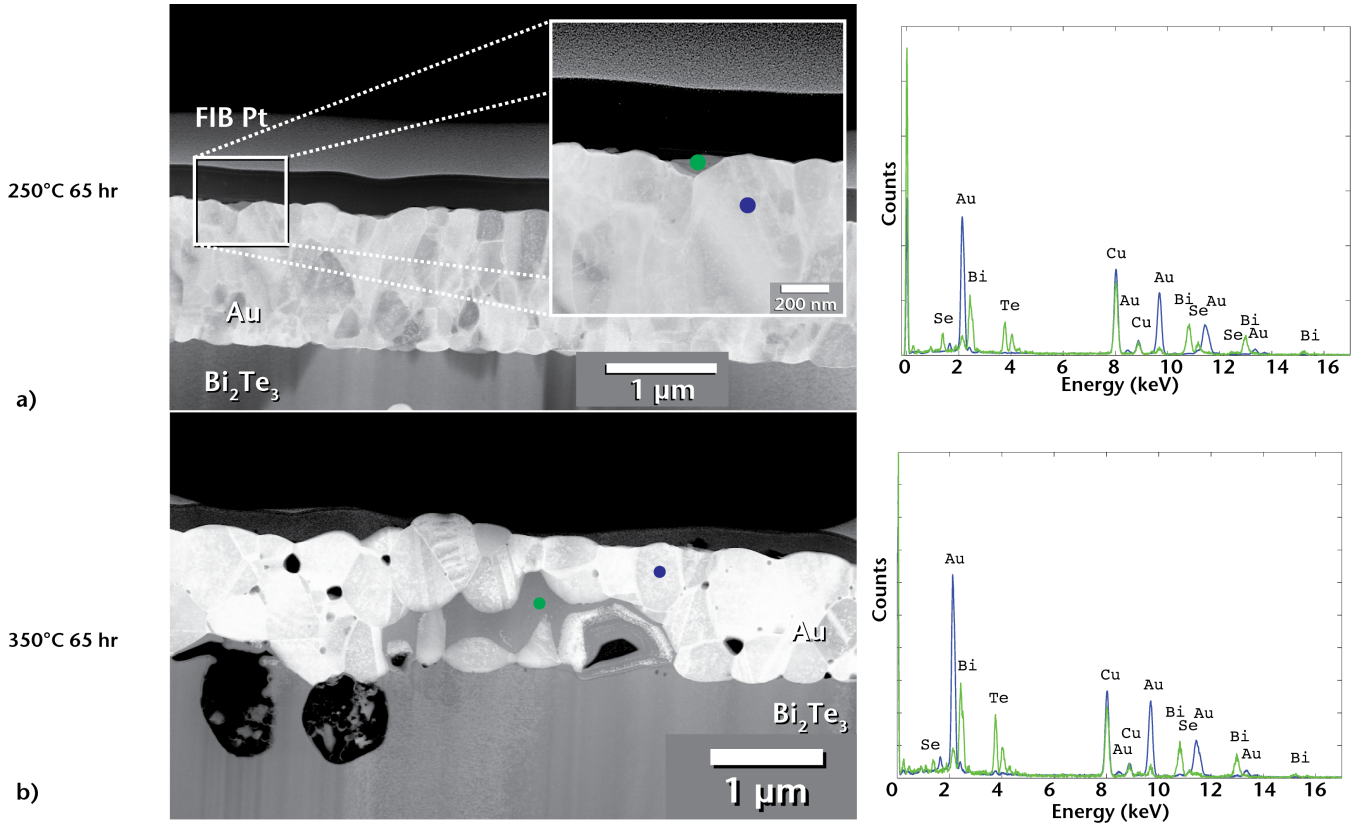


FIG. 5: In a) a HAADF STEM image shows a cross-sectional view of Au on Bi₂Te₃. Two layers of Pt are visible atop the 1 μ m thick polycrystalline Au contact pad. The inset image is a higher magnification view of the boxed region. In it, there is a feature with different contrast on the surface of the Au at a grain boundary junction. EDS analysis on this region and the neighboring Au shows that this feature is a second-phase precipitate crust containing Bi, Te, Se, and Au. It is likely that atoms from the substrate diffused along the Au grain boundaries and formed a precipitate at the surface. In b), a second phase precipitate is seen in the middle of the Au film. Again, EDS analysis shows this precipitate contains Au, Bi, Te, and Se. There are also large pores (black) in the substrate and contact.

crystalline samples, because while the formation energy for interstitials is large compared to substitutional defects, the effective formation energy for substitutional sites will be larger.

The calculations yield the formation energies for Au dopants in the perfectly crystalline Bi₂Te₃ environment, but Au-dopants will coexist alongside native defects in real Bi₂Te₃. Antisite defects are expected to be dominant, but vacancies and self-interstitials may be present [25, 38]. These various native defects will allow for different Au doping mechanisms because of the relatively small Au interstitial and substitutional defect formation energies. The processing involving deformation and intentional p- or n-type doping[39] could further alter the population and solubility of Au dopants. Diverse Cu doping locations in Bi₂Se₃, a closely related material with an identical crystal structure and a van der Waals bound Se-Se double layer[40], demonstrate a sensitive dependence on processing conditions in this system, too. Because the diffusion of Au from a contact is inherently non-equilibrium, the diffusing Au atoms in any case should not be expected to exclusively occupy the lowest energy substitutional sites.

In spite of the potential for many coexisting Au doping sites, the weak bonding and large spacing between the Te-Te double layers suggest Au diffusion through Te-Te interstitial sites in Bi₂Te₃ could be important over a range of doping and processing conditions. Experimental measurements of diffusion barriers of Au [14], Ag [16] and Cu [15] at room temperature in single crystal Bi₂Te₃ indicate the diffusion is strongly anisotropic, with an activation energy of 0.20 eV (0.45, 0.21 eV) for the in-plane direction and 0.56 eV (0.92, 0.80 eV) in the cross plane direction for Au (Ag,Cu).

We compute the Au in-plane diffusion barrier and find it is 0.18 eV, in good agreement with the experimental value of 0.20 eV [14]. The diffusion is not along a straight line connecting the adjacent interstitial sites. In the relatively open structure of the Te-Te double layer, the Au atom moves along a curved path to maximize the Te-Au distance. Fig 6. shows the pathway, viewed along the c-axis with only the equilibrium positions of the Te atoms in

	Site	Formation Energy (eV)
	Te ⁽¹⁾ -Te ⁽¹⁾ int	1.0 eV
	Bi-Te ⁽²⁾ int	1.13 eV
Te-rich condition	Au _{Bi}	0.46
	Au _{Te⁽¹⁾}	0.08
	Au _{Te⁽²⁾}	-0.09
Bi-rich condition	Au _{Bi}	0.14
	Au _{Te⁽¹⁾}	0.28
	Au _{Te⁽²⁾}	0.11
	Au _{Te⁽¹⁾} -Te int	3.00
	Au _{Te⁽²⁾} -Te int	3.42

TABLE I: Single Au-dopant formation energies. Substitutional formation energies are computed either by displacing substituted lattice atom into an adjacent interstitial site (or Au_{Te^(x)}) or by using μ_{Bi} and μ_{Te} derived assuming the system contacts reservoirs of Au and either AuTe₂ or BiTe, in the Te rich and Bi rich cases, respectively.

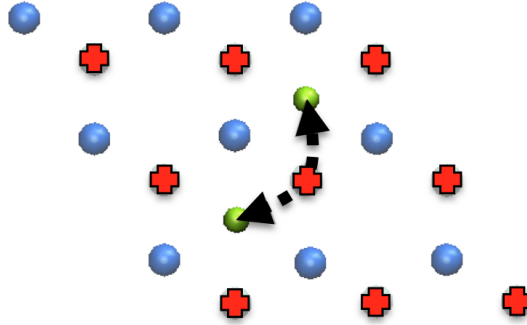


FIG. 6: Schematic illustrating the Au diffusion pathway in the Te-Te double layer plane. The Te atoms in the upper plane are shown as blue (color online) spheres and those in the lower plane are shown with red crosses. The Au atom is shown at the initial and final positions in lime green. The pathway bends upward out of the plane at its midpoint to avoid the Te atom in the lower plane.

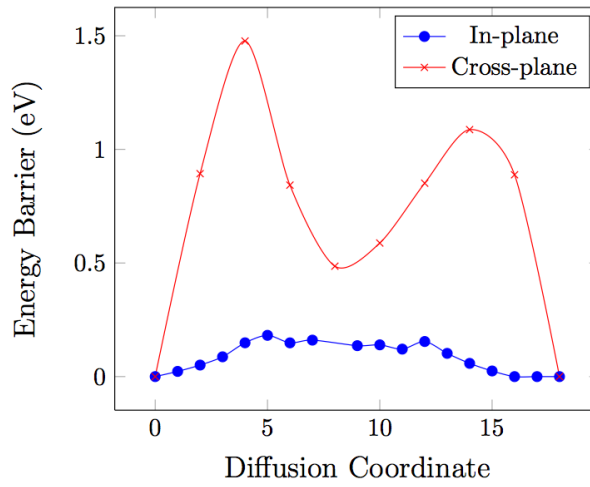


FIG. 7: Total energy as a function of position along the diffusion pathway. The initial Te-Te interstitial site corresponds to reaction coordinate 0. The energies are not symmetric about the midpoint because of the underlying asymmetry in the crystal.

the relevant double layer shown. The Te atoms slightly distort to allow the Au atom to squeeze past, with the largest distortions about one-quarter and about three-quarters of the way along the transit. Fig. 7 shows the total energy change along the diffusion pathway. The good agreement between experimental and theoretical values of the in-plane activation energy and diffusivity (in the next section) suggest the in-plane diffusion in highly crystalline samples is indeed through the interstitial mechanism discussed here.

We also compute the activation energy for diffusion in the out-of-plane direction to reach an adjacent Te-Te double layer. In this case the barrier is nearly 1.5 eV, occurring where the Au atom leaves the Te-Te double layer and pushes into the interior of the quintuple layer. The large barrier and the associated disagreement with the experimentally measured value of 0.56 eV [14] suggest other mechanisms must allow the Au atom to move in the out-of-plane direction more easily. Given the low formation energies for substitutional defects in both Bi- and Te-rich conditions, diffusion pathways involving substitutional Au intermediate states could be involved, either through vacancies or antisite defects. If such pathways are relevant they would be expected to lower the diffusion barrier because the substitutional defect would decrease the strain in the lattice. The fact that the calculated energy barrier in the cross plane direction occurs as the Au is leaving the Te-Te double layer suggests other interstitial-type paths between Te-Te double layers will encounter a similar barrier, so some pathway not accessible to the interstitial NEB method seems to be required.

In addition to the barrier height, the diffusivity itself $D = D_0 e^{E_{act}/k_B T}$ for the Au diffusing through the Bi_2Te_3 along the Te-Te double layer can be computed. Zener [41] begins from the random walk problem and suggests that $D_0 = \lambda a_0^2 \nu e^{\Delta S/k_B}$. Here λ is a geometrical factor taking into account the various paths the diffusing particle can take, a_0 is the lattice constant and ν is the vibrational frequency of the diffusing particle in the crystal potential field. In a harmonic approximation ν is approximately equal to $\sqrt{E_{act}/2ma^2}$ where E_{act} is the activation energy (barrier height), m is the Au atom mass and a is the jump distance. ΔS is an entropy term to account for the changing strain in the lattice due to the diffusing particle. It is reasonable to assume ΔS is zero, given the open Bi_2Te_3 structure and the small distortion of the lattice [15, 41]. For forward diffusion in the Bi_2Te_3 Te-Te double layer, $\lambda = 3/2$; using $a_0 = 4.38 \text{ \AA}$ and $\nu = 0.49 \times 10^{12} \text{ s}^{-1}$. Then the calculated $D_0 = 1.41 \times 10^{-3} e^{\Delta S/k_B} \text{ cm}^2/\text{s}$. The experimental value is $1.13_{-0.31}^{+0.54} \times 10^{-3} \text{ cm}^2/\text{s}$ [14], in marked agreement with the calculated value for the in-plane interstitial mechanism, suggesting this mechanism dominates transport parallel to the Te-Te double layer directions (and also that ΔS is indeed nearly zero).

Because thermoelectric devices are usually exposed to significant temperature gradients, it is useful to consider diffusion under such conditions. A temperature gradient introduces an additional term in the expression for diffusive flux \mathbf{J} in a concentration field, c .

$$\mathbf{J} = -D \frac{\partial c}{\partial \mathbf{x}} - Dc \frac{Q^*}{k_B T^2} \frac{\partial T}{\partial \mathbf{x}}. \quad (6)$$

where Q^* is the heat of transport. The second term on the right captures the Soret effect. We estimate Q^* as follows. The simple interstitial transport mechanism has a relatively low activation barrier and so we assume this mechanism dominates transport in the double layer. Because the ΔS in the diffusivity is small, and no covalent bonds are formed or broken, we further simplify the estimate of Q^* by assuming the phonon spectrum along the diffusion path is unchanging. In this approximation $-E_{act} \leq Q^* \leq E_{act}$ [42]; the limits are satisfied when the activation energy is dissipated about the initial site, or when all of it is instead carried to the final site. If the activation energy is evenly dissipated between the initial and final sites then there is no energy flux as the particle moves and $Q^* = 0$. In the present case the diffusion barrier profile, with the largest drop in energy occurring near final site, suggests energy will be mostly dissipated near the final site and so we estimate $Q^* \sim 0.18 \text{ eV}$ (the calculated diffusion barrier) for in-plane thermomigration. Experimental measurement of 0.265 eV heat of transport for Ag in Bi_2Te_3 [43] suggests the sign and magnitude of this estimate are reasonable.

To estimate the relative importance of the concentration- and temperature-driven (Soret) diffusion fluxes, we consider a model system with midpoint temperature of 200°C , a $100^\circ/\text{cm}$ temperature gradient and an initially uniform concentration at the solubility limit. Using the solubility limit measured in [14] of $1 \times 10^{18} \text{ atoms/cm}^3$ and a diffusivity of $1.36 \times 10^{-5} \text{ atoms/cm}^2 \cdot \text{s}$ the flux from the Soret term at the midpoint will be $6.37 \times 10^{13} \text{ atoms/cm}^2 \cdot \text{s}$. Using the same diffusivity and temperature concentration gradient-driven flux term at 1.66 hours from Fig. 4 is $2.5 \times 10^{12} \text{ atoms/cm}^2 \cdot \text{s}$, already an order of magnitude lower than the Soret term. Using instead our higher measured solubility limit of $6 \times 10^{18} \text{ atoms/cm}^3$ will simply multiply both flux terms by six. This estimate suggests Au fluxes from contacts into Bi_2Te_3 operating in thermoelectric modules will be largely temperature gradient-driven because the initial concentration-driven diffusion occurs so quickly.

IV. CONCLUSION

We observed diffusion of Au into n-type Bi_2Te_3 substrates and migration of Bi and Te on to the top of the Au contact material. We have calculated formation energies, diffusion barriers and diffusivity for a likely path for single Au atoms diffusing in Bi_2Te_3 . The lowest energy interstitial defect is between the Te-Te double layer. The other stable interstitial site is in the quintuple layer between the Bi and Te layer. Substitutional defects have low formation energies for Bi_2Te_3 in equilibrium with Au and either AuTe_2 or BiTe chemical reservoirs. Au substitutional defects with an adjacent displaced Bi or Te atom are found to have larger formation energies than interstitial defects due to the presence of, essentially, two defects.

Calculated values for the diffusion barrier and diffusivity along the in-plane direction agree well with experiment. The diffusion pathway winds through the Te atoms in the double layer. For diffusion in the perpendicular direction, the barrier is large and the agreement between the calculated value and experiment is poorer. The discrepancy may be due to diffusion pathways beyond the reach of the NEB method we employ.

Our results suggest that in Bi_2Te_3 near stoichiometry, if and when equilibrium is reached, the majority of Au atoms should occupy substitutional sites and any Au interstitial defects should predominately be found in the Te-Te double layer. The initial diffusion of Au should occur mainly along the in-plane direction by a mechanism involving the interstitial sites between the Te-Te double layer. When a diffusing Au atom occupies a low-energy substitutional site, it will cease moving. Because of the kinetic barrier associated with moving the displaced Te or Bi atom into the interstitial, however, it may be relatively rare for an Au atom to occupy a substitutional site. If an Au atom occupies a Te-Te double layer interstitial site, it may be expected to rapidly diffuse along the in-plane direction. We suggest the diffusion occurs in two stages. First, Au rapidly diffuses along the Te-Te double layers then quickly ceases to diffuse as the low solubility limit for interstitial Au is reached. Next, slower diffusion through an unknown vacancy- or interstitial-mediated process occurs, filling the substitutional sites. The timing of the second stage might be expected to depend sensitively on the composition of the Bi_2Te_3 ; for high quality single crystal specimens it would be exceedingly slow because of a lack of vacancies and other defects to aid the formation of substitutional Au defects, while for more highly defective polycrystalline materials the second stage would occur more quickly.

Our experiment on Au in contact with Bi_2Te_3 demonstrates the rapid diffusion of Au continuing beyond the solubility limit suggested in [14]. From a practical perspective, some of the negative consequences of Au diffusion from contacts into a thermoelectric device could be ameliorated by increasing the volume of the Au contacts so they will not be completely depleted. However, voiding may still occur at the interface (as we observe), substantially reducing the effective contact area. More concerning is that the incorporation of Au into the active thermoelectric material may gradually spoil the carefully tuned doping and transport properties. While for highly crystalline materials the second stage substitutional diffusion is expected to be kinetically slowed by the large cost of forming host interstitial - Au substitutional defect complexes, these materials might also be expected to show larger deviations in thermoelectric performance due to incorporation of Au than would more polycrystalline or off-stoichiometric samples.

ACKNOWLEDGEMENTS

Sandia National Laboratories is a multi-program laboratory managed and operated by Sandia Corporation, a wholly owned subsidiary of Lockheed Martin Corporation, for the U.S. Department of Energy's National Nuclear Security Administration under contract DE-AC04-94AL85000.

-
- [1] T. Tritt and M. A. Subramanian, MRS Bulletin **31**, 188 (2006).
 - [2] B. Poudel, Q. Hao, Y. Ma, Y. Lan, A. Minnich, B. Yu, X. Yan, D. Wang, A. Muto, D. Vashaee, et al., Science **320**, 634 (2008), <http://www.sciencemag.org/content/320/5876/634.full.pdf>, URL <http://www.sciencemag.org/content/320/5876/634.abstract>.
 - [3] K. Biswas, J. He, G. Wang, S.-H. Lo, C. Uher, V. P. Dravid, and M. G. Kanatzidis, Energy Environ. Sci. **4**, 4675 (2011), URL <http://dx.doi.org/10.1039/C1EE02297K>.
 - [4] R. J. Mehta, Y. Zhang, C. Karthik, B. Singh, R. W. Siegel, T. Borca-Tasciuc, and G. Ramanath, Nat Mater **11**, 233 (2012), URL <http://dx.doi.org/10.1038/nmat3213>.
 - [5] H. Zhang, C.-X. Liu, X.-L. Qi, X. Dai, Z. Fang, and S.-C. Zhang, Nat Phys **5**, 438 (2009), URL <http://dx.doi.org/10.1038/nphys1270>.

- [6] D. Culcer, *Physica E: Low-dimensional Systems and Nanostructures* **44**, 860 (2012), ISSN 1386-9477, <http://www.sciencedirect.com/science/article/pii/S1386947711003985>.
- [7] J. O. Jenkins, J. A. Rayne, and R. W. Ure, *Phys. Rev. B* **5**, 3171 (1972), URL <http://link.aps.org/doi/10.1103/PhysRevB.5.3171>.
- [8] J. Wiese and L. Muldrew, *Journal of Physics and Chemistry of Solids* **15**, 13 (1960), ISSN 0022-3697, URL <http://www.sciencedirect.com/science/article/pii/0022369760900949>.
- [9] P. Jones, T. E. Huber, J. Melngailis, J. Barry, M. H. Ervin, T. Zheleva, A. Nikolaeva, L. Konopko, and M. Graf, in *Thermoelectrics, 2006. ICT '06. 25th International Conference on* (2006), pp. 693–696, ISSN 1094-2734.
- [10] J. George and B. Pradeep, *Solid State Communications* **56**, 117 (1985), ISSN 0038-1098, URL <http://www.sciencedirect.com/science/article/pii/0038109885905460>.
- [11] S. Li, M. S. Toprak, H. M. A. Soliman, J. Zhou, M. Muhammed, D. Platzek, and E. Mller, *Chemistry of Materials* **18**, 3627 (2006), <http://pubs.acs.org/doi/pdf/10.1021/cm060171o>, URL <http://pubs.acs.org/doi/abs/10.1021/cm060171o>.
- [12] D. Wesolowski, R. Goeke, A. Morales, S. Goods, P. Sharma, M. Saavedra, K. Reyes-Gil, W. Neel, N. Yang, and C. Apblett, *Journal of Materials Research* **27**, 1149 (2012), URL <http://www.sciencedirect.com/science/article/pii/0038109885905460>.
- [13] W. Lin, D. Wesolowski, and C. Lee, *Journal of Materials Science: Materials in Electronics* **22**, 1313 (2011), ISSN 0957-4522, URL <http://dx.doi.org/10.1007/s10854-011-0306-0>.
- [14] J. D. Keys and H. M. Dutton, *Journal of Applied Physics* **34**, 1830 (1963), URL <http://link.aip.org/link/?JAP/34/1830/1>.
- [15] R. Carlson, *Journal of Physics and Chemistry of Solids* **13**, 65 (1960), ISSN 0022-3697, URL <http://www.sciencedirect.com/science/article/pii/002236976090127X>.
- [16] J. Keys and H. Dutton, *Journal of Physics and Chemistry of Solids* **24**, 563 (1963), ISSN 0022-3697, URL <http://www.sciencedirect.com/science/article/pii/0022369763901537>.
- [17] J. D. Keys, *Journal of Physics and Chemistry of Solids* **23**, 820 (1962), ISSN 0022-3697, URL <http://www.sciencedirect.com/science/article/pii/0022369762905401>.
- [18] M. Chitroub, S. Scherrer, and H. Scherrer, *Journal of Physics and Chemistry of Solids* **61**, 1693 (2000), ISSN 0022-3697, URL <http://www.sciencedirect.com/science/article/pii/S0022369700000317>.
- [19] P. Dato and H. Kohler, *Journal of Physics C: Solid State Physics* **17**, 3711 (1984), URL <http://stacks.iop.org/0022-3719/17/i=21/a=004>.
- [20] J.-W. Bos, F. Fauchaux, R. Downie, and A. Marcinkova, *Journal of Solid State Chemistry* **193**, 13 (2012), ISSN 0022-4596, <http://www.sciencedirect.com/science/article/pii/S0022459612001995>.
- [21] D. Rowe and C. Bhandari, *Optimization of Carrier Concentration* (CRC Press, 1995), ISBN 978-0-8493-0146-9, URL <http://dx.doi.org/10.1201/9781420049718.ch5>.
- [22] Y. S. Hor, A. Richardella, P. Roushan, Y. Xia, J. G. Checkelsky, A. Yazdani, M. Z. Hasan, N. P. Ong, and R. J. Cava, *Phys. Rev. B* **79**, 195208 (2009), URL <http://link.aps.org/doi/10.1103/PhysRevB.79.195208>.
- [23] Y. L. Chen, J. G. Analytis, J.-H. Chu, Z. K. Liu, S.-K. Mo, X. L. Qi, H. J. Zhang, D. H. Lu, X. Dai, Z. Fang, et al., *Science* **325**, 178 (2009), <http://www.sciencemag.org/content/325/5937/178.full.pdf>, URL <http://www.sciencemag.org/content/325/5937/178.abstract>.
- [24] R. Cox and H. Strack, *Solid-State Electronics* **10(12)**, 1213 (1967).
- [25] A. Hashibon and C. Elsässer, *Phys. Rev. B* **84**, 144117 (2011), URL <http://link.aps.org/doi/10.1103/PhysRevB.84.144117>.
- [26] G. Kresse and J. Furthmüller, *Phys. Rev. B* **54**, 11169 (1996), URL <http://link.aps.org/doi/10.1103/PhysRevB.54.11169>.
- [27] J. O. Jenkins, J. A. Rayne, and R. W. Ure, *Phys. Rev. B* **5**, 3171 (1972), URL <http://link.aps.org/doi/10.1103/PhysRevB.5.3171>.
- [28] S. B. Zhang and J. E. Northrup, *Phys. Rev. Lett.* **67**, 2339 (1991), URL <http://link.aps.org/doi/10.1103/PhysRevLett.67.2339>.
- [29] C. L. Ciobannu, J. Mavrogenes, N. J. Cook, and M. Shimizu, *Geo. Surver of Finland* **53** (2007), URL http://arkisto.gtk.fi/op/op53/op53_pages_15_22.pdf.
- [30] E. W. Winkler and N. F. Bright, *Solid State Communications* **2**, 293 (1964), ISSN 0038-1098, URL <http://www.sciencedirect.com/science/article/pii/0038109864905289>.
- [31] K. Reithmayer, W. Steurer, H. Schultz, and J. de Boer, *Acta Crystallographica Section B-Structural Science* **B9**, 6 (1993), URL <http://journals.iucr.org/b/issues/1993/01/00/se0099/stdsup.html>.
- [32] K. Yamana, K. Kihara, and T. Matsumoto, *Acta Crystallographica Section B* **35**, 147 (1979), URL <http://dx.doi.org/10.1107/S0567740879002788>.
- [33] J. W. G. Bos, H. W. Zandbergen, M.-H. Lee, N. P. Ong, and R. J. Cava, *Phys. Rev. B* **75**, 195203 (2007), URL <http://link.aps.org/doi/10.1103/PhysRevB.75.195203>.
- [34] P.-Y. Chevalier, *Thermochimica Acta* **130**, 15 (1988), ISSN 0040-6031, URL <http://www.sciencedirect.com/science/article/pii/0040603188870461>.
- [35] G. Mills, H. Jansson, and G. K. Schenter, *Surface Science* **324**, 305 (1995), ISSN 0039-6028, URL <http://www.sciencedirect.com/science/article/pii/0039602894007314>.
- [36] M. D. Nielsen, V. Ozolins, and J. P. Heremans, *Energy Environ. Sci.* pp. – (2013), URL <http://dx.doi.org/10.1039/>

C2EE23391F.

- [37] A. Taylor, C. Mortensen, R. Rostek, N. Nguyen, and D. C. Johnson, *Journal of Electronic Materials* **39**, 1981 (2010).
- [38] J. Hork, K. ermk, and L. Koudelka, *Journal of Physics and Chemistry of Solids* **47**, 805 (1986), ISSN 0022-3697, URL <http://www.sciencedirect.com/science/article/pii/0022369786900107>.
- [39] O. Yamashita and S. Tomiyoshi, *Journal of Applied Physics* **95**, 161 (2004), URL <http://link.aip.org/link/?JAP/95/161/1>.
- [40] A. Vako, L. Tich, J. Hork, and J. Weissenstein, *Applied physics* **5**, 217 (1974), ISSN 0340-3793, URL <http://dx.doi.org/10.1007/BF00928132>.
- [41] C. Zener, *Journal of Applied Physics* **22**, 372 (1951), URL <http://link.aip.org/link/?JAP/22/372/1>.
- [42] R. J. Asaro, D. Farkas, and Y. Kulkarni, *Acta Materialia* **56**, 1243 (2008), ISSN 1359-6454, URL <http://www.sciencedirect.com/science/article/pii/S1359645407007860>.
- [43] H. P. Dibbs and J. R. Tremblay, *Journal of Applied Physics* **39**, 2976 (1968), URL <http://link.aip.org/link/?JAP/39/2976/1>.